Robust Cascaded MPC–ASMC Control for Quadrotor Trajectory Tracking under Generalized Input Disturbances

Haidar Ahmad Ali, Amine Abadi, Aurore Gabon, and Olivier Laligant
Université Bourgogne Europe, ImViA Laboratory, Dijon, France
Emails: {ali.haidar-ahmad, amine.abadi, aurore.gabon, olivier.laligant}@u-bourgogne.fr

***Abstract*—This paper presents a cascaded Model Predictive Control–Adaptive Sliding Mode Control (MPC–ASMC) architecture for quadrotor trajectory tracking under generalized-input disturbances. The MPC outer loop generates desired accelerations, which are converted through a flatness-based mapping into hover-relative thrust and attitude references. The ASMC inner loop tracks these references and updates the robust switching gain online from the attitude tracking condition, avoiding overly conservative fixed gains. The controller is validated on the Quanser QDrone2 model in Quanser Interactive Labs using MATLAB/Simulink. Under half-sine force and torque perturbations injected at the plant input, MPC–ASMC reduces the position RMSE by 66.1%, the maximum position error by 65.1%, and the roll–pitch attitude RMSE by 52.1% compared with a cascaded MPC–SMC baseline. The results show that combining predictive translational control with adaptive robust attitude stabilization improves trajectory recovery under direct force and torque disturbances.**

***Index Terms*—Quadrotor control, Model Predictive Control, Adaptive Sliding Mode Control, trajectory tracking, disturbance rejection, QDrone2.**

I. Introduction

Quadrotors are widely used in robotics because of their agility, mechanical simplicity, and ability to perform three-dimensional motion in confined environments. However, accurate trajectory tracking remains challenging because these vehicles are nonlinear, strongly coupled, and underactuated: four rotor inputs must control six degrees of freedom [1]–[3]. Moreover, their low inertia and fast attitude dynamics make them sensitive to wind gusts, actuator perturbations, modeling errors, and payload variations.

A widely used solution is to design the controller in a cascaded structure. In this architecture, the outer loop regulates the translational motion and generates thrust and attitude references, while the inner loop tracks the attitude references and stabilizes the rotational dynamics. This decomposition is physically meaningful because quadrotor translation is produced by orienting the thrust vector through roll and pitch motion. Hence, accurate attitude tracking is essential for accurate position tracking. Several nonlinear and geometric control approaches have been proposed for quadrotor tracking and agile maneuvering [4]–[6]. These works highlight the importance of exploiting the structure of quadrotor dynamics, especially differential flatness, which allows position and yaw references to be mapped into thrust and attitude commands.

Model Predictive Control is particularly attractive for the outer loop because it can predict future tracking errors and optimize control actions over a finite horizon while handling input and rate constraints [7], [8]. For quadrotors, MPC has been shown to provide accurate trajectory tracking and good constraint-handling properties, especially for aggressive or disturbance-affected flight [9], [10]. However, an MPC outer loop alone does not eliminate the need for a fast and robust attitude controller. If the inner loop cannot track the roll and pitch commands accurately during disturbances, the commanded translational acceleration is not correctly realized by the vehicle. Therefore, the performance of the complete cascaded system depends strongly on the robustness of the attitude controller.

Sliding Mode Control is a natural candidate for the inner loop because of its robustness against bounded matched uncertainties and disturbances [11]–[13]. Classical SMC drives the system state toward a sliding manifold and maintains it there despite perturbations. However, fixed-gain SMC requires gains large enough to dominate the worst-case disturbance. This can lead to conservative control action and increased switching activity. Adaptive sliding mode strategies address this limitation by adjusting the switching gain online based on the tracking condition, improving robustness while reducing the need for large fixed gains [14], [15]. This makes adaptive SMC well suited for quadrotor attitude stabilization under time-varying force and torque disturbances.

In this paper, a robust cascaded MPC–ASMC controller is developed and validated for the Quanser QDrone2 platform [16], [17]. The proposed method keeps the predictive translational MPC structure and explicitly replaces the fixed inner-loop SMC switching gain by an adaptive gain driven by the sliding surface and tracking errors. This is the main difference from a cascaded MPC–SMC design and is practically useful when the disturbance bound is not known a priori.

The main contributions of this work are summarized as follows:

- A cascaded MPC–ASMC controller is implemented for QDrone2 trajectory tracking, where a flatness mapping

This work was supported by the EIPHI Graduate School under contract ANR-17-EURE-0002 and by the Bourgogne-Franche-Comté Region.

converts predictive acceleration commands into thrust and attitude references for the adaptive attitude loop.
- The adaptive inner loop increases the robust switching gain only when the sliding surface and attitude errors require it, improving disturbance rejection compared with a fixed-gain MPC–SMC baseline under the same disturbance scenario.

Notation

Bold lowercase symbols denote vectors, $\|\cdot\|$ is the Euclidean norm, and $\mathrm{diag}(\cdot)$ denotes a diagonal matrix. Desired variables use subscript d, tracking errors use e, estimated parameters use hats, and $i \in \{1, 2, 3\}$ denotes the roll, pitch, and yaw axes.

The remainder of this paper is organized as follows. Section II presents the QDrone2 dynamic model. Section III describes the cascaded MPC–ASMC control design and the stability analysis of the adaptive attitude loop. Section IV presents the Quanser Interactive Labs simulation setup, disturbance scenario, and comparative results. Section V concludes the paper.

II. Quadrotor Modeling

The Quanser QDrone2 is modeled as a rigid-body quadrotor evolving in an inertial frame $\mathcal{I}$ and a body-fixed frame $\mathcal{B}$. Let $\mathbf{p} = [x\ y\ z]^T$ and $\mathbf{v} = \dot{\mathbf{p}}$ denote the inertial position and velocity, while $\eta = [\phi\ \theta\ \psi]^T$ and $\omega = [p\ q\ r]^T$ denote the Euler attitude and body angular velocity. The generalized input vector applied to the vehicle is

$$GF = \begin{bmatrix} U_z & \tau_\phi & \tau_\theta & \tau_\psi \end{bmatrix}^T, \qquad \tau = \begin{bmatrix} \tau_\phi & \tau_\theta & \tau_\psi \end{bmatrix}^T. \quad (1)$$

Using the Z-Y-X Euler convention, the body-to-inertial rotation matrix is

$$R(\eta) = \begin{bmatrix} c_\psi c_\theta & c_\psi s_\theta s_\phi - s_\psi c_\phi & c_\psi s_\theta c_\phi + s_\psi s_\phi \\ s_\psi c_\theta & s_\psi s_\theta s_\phi + c_\psi c_\phi & s_\psi s_\theta c_\phi - c_\psi s_\phi \\ -s_\theta & c_\theta s_\phi & c_\theta c_\phi \end{bmatrix}, \quad (2)$$

where $c_{(\cdot)} = \cos(\cdot)$ and $s_{(\cdot)} = \sin(\cdot)$. The Euler-angle rates are related to the body angular velocity by

$$\dot{\eta} = T(\eta)\omega, \qquad T(\eta) = \begin{bmatrix} 1 & s_\phi \tan\theta & c_\phi \tan\theta \\ 0 & c_\phi & -s_\phi \\ 0 & s_\phi / c_\theta & c_\phi / c_\theta \end{bmatrix}. \quad (3)$$

The nonlinear QDrone2 dynamics are written in compact Newton–Euler form as

$$\begin{aligned} \dot{\mathbf{p}} &= \mathbf{v}, \\ \dot{\mathbf{v}} &= \frac{1}{m} R(\eta) \begin{bmatrix} 0 \\ 0 \\ U_T \end{bmatrix} - g e_3 + \frac{1}{m} d_p, \\ \dot{\eta} &= T(\eta)\omega, \\ \dot{\omega} &= J^{-1} \left(\tau - \omega \times J\omega + d_\tau \right), \end{aligned} \quad (4)$$

where m is the vehicle mass, $J = \mathrm{diag}(J_x, J_y, J_z)$ is the inertia matrix, U_T is the total collective thrust, and d_p, d_τ represent external force and torque disturbances. Since the implemented thrust command is expressed with respect to hover, the total thrust is

$$U_T = mg + U_z. \quad (5)$$

The main physical parameters used in simulation are summarized in Table I.

TABLE I
QDrone2 physical parameters used in simulation.

Parameter	Symbol	Value
Mass	m	1.504 kg
Roll inertia	J_x	$0.0177209\ \mathrm{kg\,m^2}$
Pitch inertia	J_y	$0.0169101\ \mathrm{kg\,m^2}$
Yaw inertia	J_z	$0.029448\ \mathrm{kg\,m^2}$
Roll arm length	L_ϕ	0.254 m
Pitch arm length	L_θ	0.2032 m
Yaw torque ratio	K_τ	0.01454
Gravity acceleration	g	$9.81\ \mathrm{m/s^2}$

The QDrone2 is underactuated since four generalized inputs must control six degrees of freedom. Therefore, a cascaded architecture is adopted: the outer loop generates the collective thrust and attitude references required for translational tracking, while the inner loop stabilizes the attitude dynamics and produces the torque commands.

III. Cascaded MPC–ASMC Control Design

The proposed controller combines a predictive translational outer loop with a robust adaptive attitude inner loop. The outer-loop MPC computes the acceleration command $a_c = [a_x\ a_y\ a_z]^T$ from the position and velocity tracking errors. This acceleration is mapped into the collective thrust and attitude references through a flatness transformation. The resulting command sent to the inner loop is

$$u_c = \begin{bmatrix} \phi_d & \theta_d & \psi_d & \dot{\phi}_d & \dot{\theta}_d & \dot{\psi}_d \end{bmatrix}^T. \quad (6)$$

The ASMC inner loop then generates the torque vector τ, and the plant receives the complete generalized input vector

$$GF = \begin{bmatrix} U_z & \tau_\phi & \tau_\theta & \tau_\psi \end{bmatrix}^T. \quad (7)$$

This decomposition exploits the natural time-scale separation of the quadrotor: the MPC anticipates the slower translational motion, while the ASMC enforces fast and robust attitude convergence. Since the translational acceleration is produced through the thrust direction, improved attitude tracking directly improves position tracking under external disturbances.

A. Outer-Loop MPC and Flatness Mapping

The MPC uses a discrete double-integrator prediction model for the translational states,

$$x_m = \begin{bmatrix} X & \dot{X} & Y & \dot{Y} & Z & \dot{Z} \end{bmatrix}^T, \qquad u_m = \begin{bmatrix} a_x & a_y & a_z \end{bmatrix}^T. \quad (8)$$

The compact prediction model is

$$x_{m,k+1} = A_d x_{m,k} + B_d u_{m,k}, \quad (9)$$

where A_d and B_d are obtained from the discretization of the translational double-integrator dynamics. The MPC sampling time and prediction horizon are selected as $T_s = 0.02$ s and $N = 20$, giving $3N = 60$ acceleration decision variables. In this simulation study the QP was solved on a desktop MATLAB/Simulink setup; embedded worst-case timing is therefore not claimed and will be profiled in physical implementation.

At each sampling instant, the MPC solves the finite-horizon quadratic program

$$\begin{aligned} \min_{\mathbf{u}} \quad & \sum_{i=1}^{N} \left(\|\mathbf{p}_{k+i} - \mathbf{p}^r_{k+i}\|^2_{Q_p} + \|\mathbf{v}_{k+i} - \mathbf{v}^r_{k+i}\|^2_{Q_v} \right) \\ & + \sum_{i=0}^{N-1} \left(\|u_{m,k+i}\|^2_R + \|\Delta u_{m,k+i}\|^2_{R_\Delta} \right) \end{aligned} \tag{10}$$

subject to acceleration and acceleration-rate constraints. Only the first optimal acceleration command is applied, and the optimization is repeated at the next sampling instant.

The acceleration command is converted into thrust and attitude references. Defining

$$a_T = \begin{bmatrix} a_x & a_y & g + a_z \end{bmatrix}^T, \tag{11}$$

the total thrust and hover-relative thrust command are

$$U_T = m\|a_T\|, \qquad U_z = U_T - mg. \tag{12}$$

For a desired yaw angle ψ_d, the pitch and roll references are computed as

$$\begin{aligned} \theta_d &= \operatorname{atan2}\left(a_x \cos\psi_d + a_y \sin\psi_d,\ g + a_z\right), \\ \phi_d &= \sin^{-1}\left(\frac{a_x \sin\psi_d - a_y \cos\psi_d}{\sqrt{a_x^2 + a_y^2 + (g + a_z)^2}} \right). \end{aligned} \tag{13}$$

The reference rates $\dot{\phi}_d$ and $\dot{\theta}_d$ are obtained from the time variation of the saturated attitude references, while ψ_d and $\dot{\psi}_d$ are provided as yaw commands.

B. Inner-Loop Adaptive Sliding Mode Control

The desired attitude is $\eta_d = [\phi_d\ \theta_d\ \psi_d]^T$. The commanded Euler-rate vector is converted into the desired body-rate vector $\omega_d = [p_d\ q_d\ r_d]^T$ as

$$\begin{aligned} p_d &= \dot{\phi}_d - \dot{\psi}_d \sin\theta_d, \\ q_d &= \dot{\theta}_d \cos\phi_d + \dot{\psi}_d \sin\phi_d \cos\theta_d, \\ r_d &= -\dot{\theta}_d \sin\phi_d + \dot{\psi}_d \cos\phi_d \cos\theta_d. \end{aligned} \tag{14}$$

The attitude and angular velocity tracking errors are

$$e_\eta = \eta - \eta_d, \qquad e_\omega = \omega - \omega_d. \tag{15}$$

The sliding surface is selected as

$$s = e_\omega + \Lambda e_\eta, \qquad \Lambda = \operatorname{diag}(\lambda_\phi, \lambda_\theta, \lambda_\psi) > 0. \tag{16}$$

When $s = 0$, the reduced attitude error dynamics satisfy $\dot{e}_\eta + \Lambda e_\eta = 0$, which gives exponential convergence of the attitude tracking error.

Let

$$C(\omega) = \omega \times J\omega. \tag{17}$$

The implemented ASMC torque is written as

$$\tau = C(\omega) + J\left[-\Lambda e_\omega - K_1 s - K_a(t)\operatorname{sat}_\varphi(s)\right], \tag{18}$$

where $K_1 > 0$ is a diagonal stabilizing gain and $\operatorname{sat}_\varphi(\cdot)$ is a component-wise saturation function. The adaptive switching gain is

$$K_a(t) = \operatorname{diag}(K_{2,1} + \hat{\gamma}_1,\ K_{2,2} + \hat{\gamma}_2,\ K_{2,3} + \hat{\gamma}_3), \tag{19}$$

where $K_{2,i} > 0$ are nominal robust gains. The adaptive uncertainty estimate is

$$\hat{\gamma}_i = \hat{a}_{0,i} + \hat{a}_{1,i}|e_{\eta,i}| + \hat{a}_{2,i}|e_{\omega,i}|, \qquad i = 1, 2, 3. \tag{20}$$

The adaptation law is chosen as

$$\begin{aligned} \dot{\hat{a}}_{0,i} &= \rho_{0,i}|s_i|, \\ \dot{\hat{a}}_{1,i} &= \rho_{1,i}|s_i||e_{\eta,i}|, \\ \dot{\hat{a}}_{2,i} &= \rho_{2,i}|s_i||e_{\omega,i}|, \end{aligned} \tag{21}$$

with positive adaptation gains $\rho_{0,i}$, $\rho_{1,i}$, and $\rho_{2,i}$. These gains were selected manually after nominal gain tuning. The final values used in simulation were $\rho_\phi = (0.05, 0.70, 0.07)$, $\rho_\theta = (0.07, 0.70, 0.07)$, and $\rho_\psi = (2.15, 1.10, 0.50)$. Larger values improved recovery but increased torque activity, while smaller values slowed disturbance rejection.

C. Stability Analysis

Assumption 1. *The desired attitude trajectory and its derivatives are bounded. The inertia matrix J is symmetric positive definite, and the attitude representation remains away from Euler-angle singularities.*

Assumption 2. *The normalized matched rotational uncertainty $\bar{\Delta}$ is bounded. For each axis, there exist unknown positive constants $a^*_{0,i}$, $a^*_{1,i}$, and $a^*_{2,i}$ such that*

$$|\bar{\Delta}_i| \le \gamma^*_i = a^*_{0,i} + a^*_{1,i}|e_{\eta,i}| + a^*_{2,i}|e_{\omega,i}|, \qquad i = 1, 2, 3. \tag{22}$$

Theorem 1. *Under Assumptions 1 and 2, the ASMC law* (18) *with the adaptation law* (21) *guarantees bounded sliding and adaptive signals and drives the sliding surface to a neighborhood of the origin. In the ideal switching case,* $\operatorname{sat}_\varphi(s) = \operatorname{sgn}(s)$*, the sliding surface converges asymptotically to zero.*

Proof. Using (4), (16), and (18), the closed-loop sliding dynamics can be written in acceleration-level form as

$$\dot{s} = -K_1 s - K_a(t)\operatorname{sat}_\varphi(s) + \bar{\Delta}, \tag{23}$$

where $\bar{\Delta}$ collects the matched rotational disturbances and bounded reference-dependent residual terms after inertia normalization.

Consider the Lyapunov candidate

$$V = \frac{1}{2}s^T s + \frac{1}{2}\sum_{i=1}^{3}\sum_{j=0}^{2} \frac{\tilde{a}^2_{j,i}}{\rho_{j,i}}, \qquad \tilde{a}_{j,i} = a^*_{j,i} - \hat{a}_{j,i}. \tag{24}$$

Since $\rho_{j,i} > 0$, V is positive definite with respect to the sliding surface and the parameter estimation errors.

For the ideal switching case, $\mathrm{sat}_\varphi(s) = \mathrm{sgn}(s)$. Differentiating (24) and substituting (23) gives

$$\dot{V} = -s^T K_1 s - s^T K_a(t)\mathrm{sgn}(s) + s^T \bar{\Delta} - \sum_{i=1}^{3}\sum_{j=0}^{2} \frac{\tilde{a}_{j,i}}{\rho_{j,i}} \dot{\hat{a}}_{j,i}. \tag{25}$$

Using $K_a(t) = \mathrm{diag}(K_{2,i} + \hat{\gamma}_i)$, $s_i \mathrm{sgn}(s_i) = |s_i|$, and $|s_i \bar{\Delta}_i| \leq \gamma_i^* |s_i|$, one obtains

$$\begin{aligned} \dot{V} \leq & -s^T K_1 s - \sum_{i=1}^{3} K_{2,i}|s_i| + \sum_{i=1}^{3}(\gamma_i^* - \hat{\gamma}_i)|s_i| \\ & - \sum_{i=1}^{3}\sum_{j=0}^{2} \frac{\tilde{a}_{j,i}}{\rho_{j,i}} \dot{\hat{a}}_{j,i}. \end{aligned} \tag{26}$$

From (20) and (22),

$$\gamma_i^* - \hat{\gamma}_i = \tilde{a}_{0,i} + \tilde{a}_{1,i}|e_{\eta,i}| + \tilde{a}_{2,i}|e_{\omega,i}|. \tag{27}$$

Substituting the adaptive laws (21) into (26) cancels the uncertainty-estimation terms, yielding

$$\dot{V} \leq -s^T K_1 s - \sum_{i=1}^{3} K_{2,i}|s_i| \leq 0. \tag{28}$$

Therefore, $V(t)$ is non-increasing, and the sliding surface and adaptive parameter estimation errors are bounded. Moreover, $s \in L_2 \cap L_\infty$. Since $\dot{s}$ is bounded under Assumption 1 and the boundedness of the closed-loop signals, Barbalat's lemma gives

$$\lim_{t\to\infty} s(t) = 0 \tag{29}$$

for the ideal switching case.

From $s = e_\omega + \Lambda e_\eta$, the reduced-order dynamics on the sliding surface are

$$\dot{e}_\eta + \Lambda e_\eta = 0. \tag{30}$$

Since Λ is positive definite, the attitude tracking error converges exponentially to zero, and the angular velocity tracking error also converges to zero.

When the saturation function is used, the discontinuous switching law is replaced by a boundary layer. In this implemented case, practical stability is obtained. Component-wise, if the boundary layer enforces $|s_i| \leq \varphi_i$ after transients, then the reduced error dynamics $\dot{e}_{\eta,i} + \lambda_i e_{\eta,i} = s_i$ give the ultimate bound

$$\limsup_{t\to\infty} |e_{\eta,i}(t)| \leq \frac{\varphi_i}{\lambda_i}, \qquad i = 1, 2, 3. \tag{31}$$

Thus, smaller φ_i improves the final tracking bound but may increase chattering. □

TABLE II
GENERALIZED-INPUT DISTURBANCES APPLIED DURING SIMULATION.

Channel	Symbol	Time	Amplitude
Thrust	U_z	25 s	3.25 N
Roll torque	τ_ϕ	30 s	1.30 N m
Pitch torque	τ_θ	40 s	1.30 N m

IV. Simulation Validation and Results

The proposed control architecture was validated on the Quanser QDrone2 model using the Quanser Interactive Labs simulation environment. The complete closed-loop system was implemented in MATLAB/Simulink, where the outer-loop MPC generated the translational acceleration, thrust, and attitude references, while the inner loop produced the torque commands applied to the plant.

To isolate the contribution of the adaptive attitude controller, two configurations were tested under the same plant model, outer-loop MPC, reference trajectory, and disturbance profile: **MPC–SMC**, with a classical fixed-gain SMC attitude inner loop, and **MPC–ASMC**, with the proposed adaptive SMC attitude inner loop. The SMC baseline used the same sliding surface and boundary layer; its switching gains were tuned on the same disturbance scenario until the RMSE no longer improved without increasing torque peaks and switching activity. Therefore, the comparison evaluates the adaptive inner-loop effect rather than a different outer-loop design.

The QDrone2 was commanded to track a single smooth three-dimensional Bezier trajectory. The trajectory starts at $t_s = 20$ s, lasts $t_f = 50$ s, reaches an altitude of approximately 1.5 m, and ends at

$$p_f = \begin{bmatrix} 3 & 4 & 0 \end{bmatrix}^T. \tag{32}$$

The reference was generated using an 11th-order Bezier polynomial for each axis, providing smooth position and velocity commands for the outer-loop MPC.

Robustness was evaluated by injecting disturbances directly at the generalized input level, after the controller output and before the QDrone2 plant:

$$GF_{\mathrm{plant}} = GF_{\mathrm{ctrl}} + dGF, \qquad GF = \begin{bmatrix} U_z & \tau_\phi & \tau_\theta & \tau_\psi \end{bmatrix}^T. \tag{33}$$

Here, U_z is the thrust force in newtons, while τ_ϕ, τ_θ, and τ_ψ are body torques in newton-meters. The applied half-sine disturbances have a duration of $T_d = 1.5$ s and are summarized in Table II.

Unlike measurement noise, these disturbances directly perturb the plant input. The thrust pulse is about 22% of hover thrust ($mg \simeq 14.75$ N), while the roll and pitch pulses correspond to differential thrust levels of approximately 5.1 N and 6.4 N using the QDrone2 arm lengths. They were selected as severe but bounded input disturbances that produce visible transients without causing loss of control.

A. Outer-Loop Trajectory Tracking

Fig. 1 shows the outer-loop tracking performance under the applied generalized-input disturbances. The figure includes

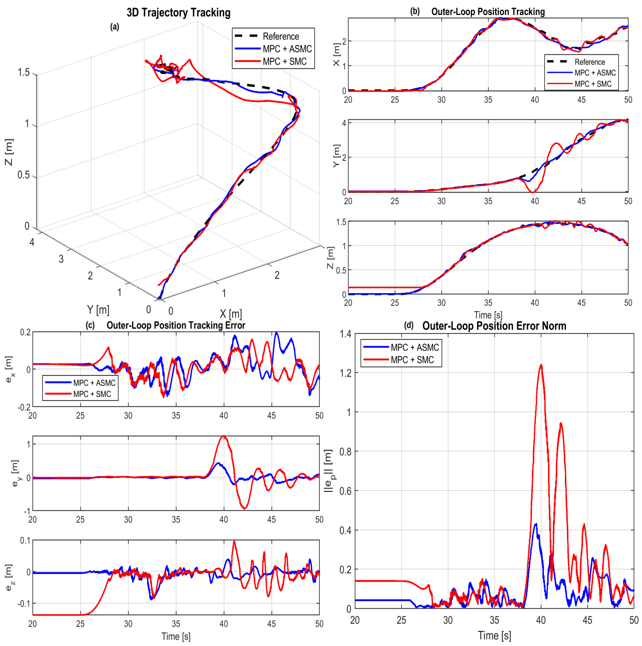

Fig. 1. Outer-loop tracking under generalized-input disturbances: (a) three-dimensional Bezier trajectory tracking, (b) position tracking response, (c) position tracking errors, and (d) position error norm. The same reference trajectory and disturbance profile are applied to both MPC–SMC and MPC–ASMC.

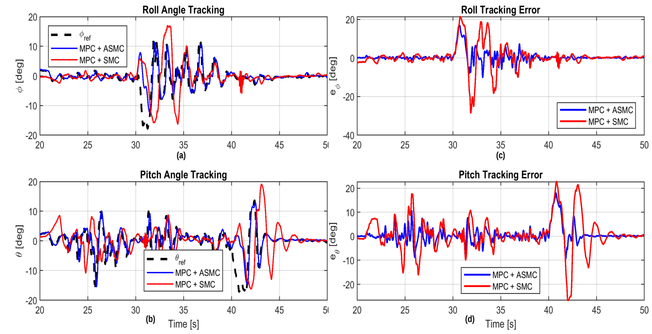

Fig. 2. Inner-loop attitude tracking under generalized-input disturbances: (a) roll angle tracking, (b) pitch angle tracking, (c) roll tracking error, and (d) pitch tracking error.

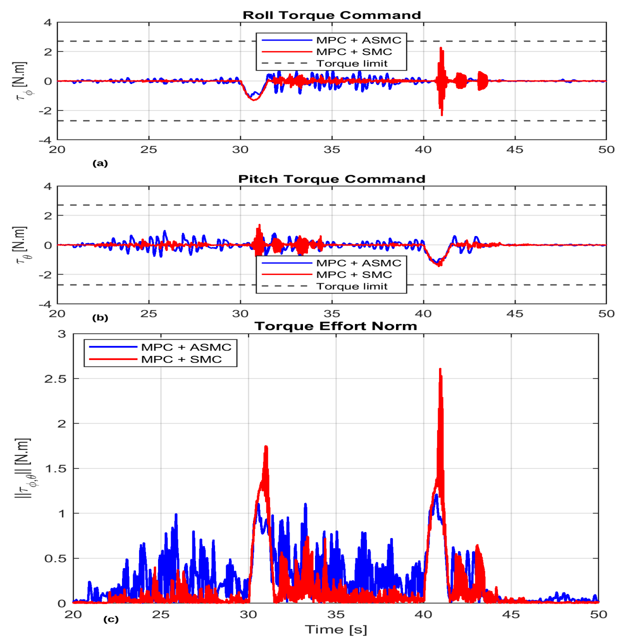

Fig. 3. Inner-loop torque response under generalized-input disturbances: (a) roll torque command, (b) pitch torque command, and (c) roll–pitch torque effort norm.

the three-dimensional Bezier trajectory, the axis-wise position tracking response, the position tracking errors, and the position error norm. Both controllers are able to follow the reference trajectory; however, the MPC–ASMC response remains closer to the desired path during the disturbance intervals and shows faster recovery after the perturbations.

This improvement is a direct consequence of the adaptive attitude loop. Since the outer-loop MPC generates translational accelerations that are realized through thrust and attitude references, any improvement in roll and pitch tracking improves the effective translational response of the quadrotor.

B. Inner-Loop Attitude Response

Fig. 2 presents the roll and pitch tracking performance of the inner loop. The roll and pitch references are generated by the MPC through the flatness mapping and must be accurately tracked by the attitude controller to preserve the desired thrust direction. The fixed-gain SMC controller exhibits larger deviations during the roll and pitch disturbance intervals, while the ASMC controller reduces the tracking error and recovers more rapidly.

C. Torque Response and Adaptive Behavior

The torque response is shown in Fig. 3. The torque effort increases around the disturbance intervals, showing that the attitude controller actively compensates for the perturbations injected at the generalized-input level. Compared with MPC–SMC, the MPC–ASMC controller limits the largest torque demand while maintaining better tracking performance, especially during the roll and pitch disturbance events.

Fig. 4 highlights the adaptive mechanism of the ASMC inner loop. The plotted effective gain corresponds to $K_{\text{eff},i} = K_{2,i} + \hat{\gamma}_i$, with $i \in \{\phi, \theta\}$, where $K_{2,i}$ is the nominal switching gain and $\hat{\gamma}_i$ is the adaptive uncertainty estimate. The effective gains increase when the sliding surfaces become larger, especially around the roll and pitch disturbance intervals. After the perturbations are rejected, the sliding surfaces return close to zero, confirming that the adaptive law increases the robust control action only when required by the attitude tracking condition.

D. Quantitative Performance Comparison

The tracking performance was quantified using the position RMSE, position MAE, maximum position error, and roll–pitch attitude RMSE. The position error norm is defined as

$$e_p(k) = \|\mathbf{p}_k - \mathbf{p}_{d,k}\|. \tag{34}$$

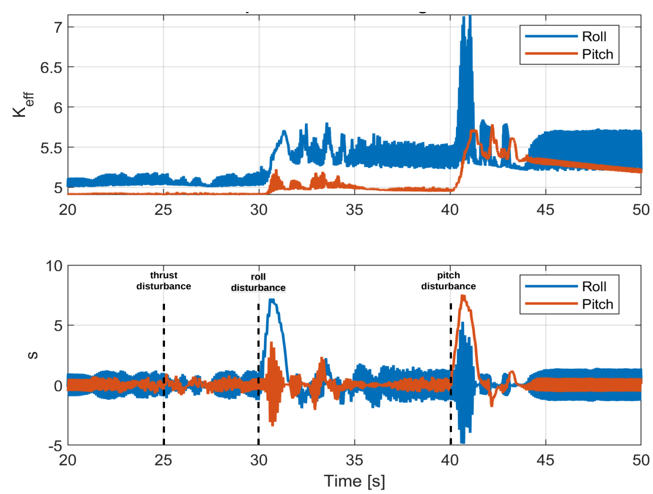

Fig. 4. Adaptive ASMC response under generalized-input disturbances: effective gains and sliding surfaces s for roll and pitch.

TABLE III
PERFORMANCE COMPARISON UNDER GENERALIZED-INPUT DISTURBANCES.

Metric	MPC–SMC	MPC–ASMC
Position RMSE [m]	0.336	**0.114**
Position MAE [m]	0.204	**0.080**
Maximum position error [m]	1.239	**0.432**
Roll–pitch attitude RMSE [deg]	9.33	**4.47**

The corresponding position metrics are

$$RMSE_p = \sqrt{\frac{1}{N_s}\sum_{k=1}^{N_s} e_p^2(k)}, \qquad MAE_p = \frac{1}{N_s}\sum_{k=1}^{N_s} e_p(k). \tag{35}$$

The roll–pitch attitude RMSE is evaluated using

$$RMSE_{\phi\theta} = \sqrt{RMSE_\phi^2 + RMSE_\theta^2}. \tag{36}$$

As shown in Table III, the proposed MPC–ASMC controller reduces the total position RMSE from 0.336 m to 0.114 m, corresponding to an improvement of approximately 66.1%. The maximum position error is reduced by approximately 65.1%, while the roll–pitch attitude RMSE is reduced by approximately 52.1%. These results confirm that the adaptive attitude loop significantly improves disturbance rejection and trajectory recovery while preserving bounded control effort.

Overall, the validation demonstrates that the proposed cascaded MPC–ASMC architecture combines the predictive tracking capability of MPC with the robustness of adaptive sliding mode attitude control. The MPC provides smooth thrust and attitude references, while the ASMC inner loop improves attitude stabilization under direct force and torque perturbations, resulting in more accurate and robust QDrone2 trajectory tracking.

V. Conclusion

This paper presented a cascaded MPC–ASMC architecture for robust QDrone2 trajectory tracking under generalized-input disturbances. The outer-loop MPC generated acceleration commands that were converted through a flatness-based mapping into hover-relative thrust and attitude references, while the ASMC inner loop produced the torque commands needed for attitude tracking and disturbance rejection.

Validation in Quanser Interactive Labs/MATLAB–Simulink showed that replacing the fixed-gain SMC inner loop with ASMC improves trajectory recovery under the same Bezier reference and generalized-input disturbance profile. MPC–ASMC reduced the position RMSE by 66.1%, the maximum position error by 65.1%, and the roll–pitch attitude RMSE by 52.1% compared with MPC–SMC, confirming that adaptive robust attitude stabilization helps the outer MPC maintain a more accurate thrust direction during force and torque perturbations.

References

[1] R. Mahony, V. Kumar, and P. Corke, “Multirotor aerial vehicles: Modeling, estimation, and control of quadrotor,” *IEEE Robotics & Automation Magazine*, vol. 19, no. 3, pp. 20–32, 2012.
[2] S. Bouabdallah, P. Murrieri, and R. Siegwart, “Design and control of an indoor micro quadrotor,” in *Proc. IEEE International Conference on Robotics and Automation (ICRA)*, 2004, pp. 4393–4398.
[3] G. M. Hoffmann, H. Huang, S. L. Waslander, and C. J. Tomlin, “Quadrotor helicopter flight dynamics and control: Theory and experiment,” in *Proc. AIAA Guidance, Navigation and Control Conference*, 2007.
[4] T. Lee, M. Leok, and N. H. McClamroch, “Geometric tracking control of a quadrotor UAV on SE(3),” in *Proc. IEEE Conference on Decision and Control (CDC)*, 2010, pp. 5420–5425.
[5] D. Mellinger and V. Kumar, “Minimum snap trajectory generation and control for quadrotors,” in *Proc. IEEE International Conference on Robotics and Automation (ICRA)*, 2011, pp. 2520–2525.
[6] M. Faessler, A. Franchi, and D. Scaramuzza, “Differential flatness of quadrotor dynamics subject to rotor drag for accurate tracking of high-speed trajectories,” *IEEE Robotics and Automation Letters*, vol. 3, no. 2, pp. 620–626, 2018.
[7] D. Q. Mayne, J. B. Rawlings, C. V. Rao, and P. O. M. Scokaert, “Constrained model predictive control: Stability and optimality,” *Automatica*, vol. 36, no. 6, pp. 789–814, 2000.
[8] J. B. Rawlings, D. Q. Mayne, and M. Diehl, *Model Predictive Control: Theory, Computation, and Design*, 2nd ed. Madison, WI, USA: Nob Hill Publishing, 2017.
[9] M. Kamel, M. Burri, and R. Siegwart, “Linear vs nonlinear MPC for trajectory tracking applied to rotary wing micro aerial vehicles,” *IFAC-PapersOnLine*, vol. 50, no. 1, pp. 3463–3469, 2017.
[10] S. Sun, A. Romero, P. Foehn, E. Kaufmann, and D. Scaramuzza, “A comparative study of nonlinear MPC and differential-flatness-based control for quadrotor agile flight,” *IEEE Transactions on Robotics*, vol. 38, no. 6, pp. 3357–3373, 2022.
[11] V. I. Utkin, “Variable structure systems with sliding modes,” *IEEE Transactions on Automatic Control*, vol. 22, no. 2, pp. 212–222, 1977.
[12] C. Edwards and S. K. Spurgeon, *Sliding Mode Control: Theory and Applications*. London, U.K.: Taylor & Francis, 1998.
[13] Y. Shtessel, C. Edwards, L. Fridman, and A. Levant, *Sliding Mode Control and Observation*. New York, NY, USA: Birkhäuser, 2014.
[14] J.-J. E. Slotine and W. Li, *Applied Nonlinear Control*. Englewood Cliffs, NJ, USA: Prentice Hall, 1991.
[15] A. Eltayeb, M. F. Rahmat, M. A. M. Basri, and M. A. Mohammed, “Robust adaptive sliding mode control design for quadrotor unmanned aerial vehicle trajectory tracking,” *International Journal of Computing and Digital Systems*, vol. 9, no. 2, pp. 249–257, 2020.
[16] Quanser, “QDrone 2,” Quanser Inc. [Online]. Available: https://www.quanser.com/products/qdrone-2/
[17] Quanser, “QDrone 2: Quanser Interactive Labs API Documentation,” Quanser Inc. [Online]. Available: https://qlabs.quanserdocs.com/en/latest/Objects/qdrone2_library.html